SLAC-PUB-3162
TUHEL 83-7
July 1983
(T/E)

INCLUSIVE PHOTOPRODUCTION OF NEUTRAL STRANGE PARTICLES AT 20 GeV*

SLAC Hybrid Facility Photon Collaboration

K. Abe[m], T.C. Bacon[e], J. Ballam[k], A.V. Bevan[e], H.H. Bingham[o], J.E. Brau[q], K. Braune[k†], D. Brick[b], W.M. Bugg[q], J. Butler[k], W. Cameron[e], J.T. Carroll[k], C.V. Cautis[k‡], J.S. Chima[e], H.O. Cohn[i], D.C. Colley[a], G. T. Condo[q], S. Dado[l], R. Diamond[d], R. Erickson[k], T. Fieguth[k], R.C. Field[k], B. Franek[j], N. Fujiwara[h], K. Furuno[m], R. Gearhart[k], D. Gershoni[l] J. J. Goldberg[k§], G.P. Gopal[j], A.T. Goshaw[c], E.S. Hafen[g], G. Hall[e], E.R. Hancock[j], T. Handler[q], H.J. Hargis[q], P. Haridas[g], E.L. Hart[q], K. Hasegawa[m], T. Hayashino[m], I. Hideta[m], R. I. Hulsizer[g], M. Jobes[a], G.E. Kalmus[j], D.P. Kelsey[j], J. Kent[o], T. Kitagaki[m], A. Levy[p], P. W. Lucas[c], W.A. Mann[n], R. Merenyi[n], R. Milburn[n], C. Milstene[p], K.C. Moffeit[k], J.J. Murray[k], A. Napier[n], S. Noguchi[h], F. Ochiai[f], S. O'Neale[a], Y. Ohtani[m], A.P.T. Palounek[c], I.A. Pless[g], P. Rankin[e], A.H. Rogers[q], E. Ronat[r], H. Rudnicka[b], H. Sagawa[m], T. Sato[f], J. Schneps[n], J. Shank[o], A.M. Shapiro[b], R. Sugahara[f], A. Suzuki[f¶], K. Takahashi[f], K. Tamai[m], S. Tanaka[m], S. Tether[g], W.D. Walker[c], M. Widgoff[b], C.G. Wilkins[a], S. Wolbers[o], C.A. Woods[e], A. Yamaguchi[m], R.K. Yamamoto[g], S. Yamashita[h], Y. Yoshimura[f], G.P. Yost[o], H. Yuta[m]

Submitted to Physical Review D

---

a. Birmingham University, Birmingham, England
b. Brown University, Providence, Rhode Island, USA
c. Duke University, Durham, North Carolina, USA
d. Florida State University, Tallahassee, Florida, USA
e. Imperial College, London, England
f. KEK, Oho-machi, Tsukuba-gun, Ibaraki, Japan
g. Massachusetts Institute of Technology, Cambridge, Massachusetts, USA
h. Nara Womens University, Nara, Japan
i. ORNL, Oak Ridge, Tennessee, USA
j. Rutherford Appleton Laboratory, Didcot, England
k. Stanford Linear Accelerator Center, Stanford University, Stanford, California, USA
l. Technion-Israel Institute of Technology, Haifa, Israel
m. Tohoku University, Sendai, Japan
n. Tufts University, Medford, Massachusetts, USA
o. University of California, Berkeley, California, USA
p. University of Tel Aviv, Tel Aviv, Israel
q. University of Tennessee, Knoxville, Tennessee, USA
r. Weizmann Institute, Rehovot, Israel

ABSTRACT

We have studied inclusive production of K_s^0, Λ, and $\bar{\Lambda}$ particles in 20 GeV γp interactions and have found features similar to those observed in both hadronic and leptonic interactions. The production cross sections, charged particle multiplicities, and average Λ polarization are reported. Inclusive distributions of x and p_T are shown and discussed in terms of quark fragmentation models. Production cross sections for $K^*(890)$ and $\Sigma^*(1385)$ are also reported.

1. Introduction

Inclusive production of neutral strange particles has been studied with a variety of hadron[1–11] and lepton[12–19] beams. The only inclusive data on neutral strange particle production with photons, however, come from bubble chamber experiments at 5.8 GeV[20] and at 9.3 GeV[21], and a more recent experiment at the CERN Omega spectrometer using a bremsstrahlung beam[22].

In this paper, we present results on K^0_s, Λ, and $\bar{\Lambda}$ production with a monoenergetic photon beam incident on the hydrogen-filled bubble chamber of the SLAC Hybrid Facility. The nearly full acceptance and the visual detection of secondary V^0 decays make the bubble chamber particularly well suited to the study of these particles. In most cases, neutral V's can be uniquely identified by their decay kinematics. Longitudinal and transverse momentum distributions and other features of the production mechanisms of these particles are reported here and compared to other inclusive data. We also report results on the $\Sigma^*(1385)$ and the first inclusive photoproduction cross sections for the $K^*(890)$.

2. Experimental Procedure

Some 2.4 million pictures have been taken with the SLAC 1 m bubble chamber exposed to a photon beam. This beam was produced by collimating the back-scattered photons from the interaction of ultraviolet light from a frequency-quadrupled Nd:YAG laser with a 30 GeV electron beam, resulting in a spectrum peaked at 20 GeV with a full width at half maximum of about 2 GeV[23]. The flux was typically 20 photons per pulse. Processing of the film is in progress at this time. The results presented here are based on about 20 percent of the film for which the processing has been completed.

The apparatus is shown in Fig. 1. Downstream of the bubble chamber were 11 planes of multiwire proportional chambers grouped in four stations, two gas filled Cerenkov counters[24] which provided π/Kp discrimination above 3.1 GeV/c, and a lead glass wall[23]. The Cerenkov counters and lead glass wall data were not used in the analysis presented here. Because the photon beam produced $e^{\pm}$ pairs as it traversed the apparatus, all of the detectors downstream of the bubble chamber were made insensitive in the narrow region of dense electromagnetic background.

The cameras were triggered by the passage of any charged particle through the first three PWC stations, or by a sufficient energy deposition in the lead glass wall. Approximately one picture out of five contained a usable hadronic interaction. In order to study the triggering efficiency, we took an untriggered picture on every 50th frame. From these pictures, it was determined that we trigger on 88 $\pm$ 3 percent of the total hadronic cross section, and that this efficiency is nearly independent of the event topology. Furthermore, Monte Carlo studies show that the triggering efficiency should be independent of the momentum of any V^0 in the event. We take this to be strictly true in the analyses that follow. The efficiency was also checked by measuring the incident photon flux with a lead-lucite beam-stop shower counter, as well as with a pair spectrometer beam monitor upstream of the bubble chamber. With these devices, we directly measured an integrated flux corresponding to a total cross section of 89 $\pm$ 9 μb for this data sample. When compared to the published value[25] of 115 $\pm$ 2 μb, this indicates an overall efficiency (including scanning and measuring losses) of 77 $\pm$ 8 percent. The error on this efficiency is due almost entirely to systematic uncertainties in the calibration of the pair spectrometer and the beam-stop counter, and in the density of the liquid hydrogen during the bubble chamber expansion cycle. These systematic effects cancel in the results reported below, because the cross sections and

inclusive distributions are derived from ratios of strange particles to total hadronic events.

The analyses that follow are based on 97,100 hadronic interactions that occurred within a cleanly defined primary fiducial volume. A minimum decay length cut of 2.0 mm was imposed on all neutral V vertices to ensure high detection efficiency[26], and a secondary fiducial volume was defined so that all decay products had measurable track lengths of at least 7 cm. 14200 neutral V's passed these initial cuts.

Each of the observed neutral V's was checked against four hypotheses:

$$\gamma p \rightarrow e^+ e^- p \tag{1}$$

$$K_s^0 \rightarrow \pi^+ \pi^- \tag{2}$$

$$\Lambda \rightarrow p \pi^- \tag{3}$$

$$\bar{\Lambda} \rightarrow \bar{p}\, \pi^+ \tag{4}$$

Three-constraint fits were attempted by a kinematic fitting program, requiring that the reconstructed momentum vector of the neutral particle point to the primary interaction vertex with a fit probability greater than 0.1 percent. 79 percent of the neutral V's (including γ conversions) were uniquely identified by these fits, leaving 10 percent with two or more successful fits, and 11 percent with no acceptable fits.

As a first step in resolving the ambiguous decays, any neutral V that fitted the γ conversion hypothesis (reaction 1) with an invariant mass less than 30 MeV/c^2 and had a positive decay track with transverse momentum less than 10 MeV/c was classified as a γ and eliminated from further consideration. We estimate that fewer than 1 percent of the neutral strange particles were lost by misidentification as γ conversions. V^0's with identifications ambiguous among two or more strange particle hypotheses were each assigned a unique identification based on the following procedure. Each K_s^0/Λ ambiguity was resolved as a K_s^0 if the χ^2 probability of the K_s^0 fit was greater than

0.70 and was greater than that of the Λ fit; otherwise, it was called a Λ. Similarly, each $K_s^0/\bar{\Lambda}$ ambiguity was resolved as a $\bar{\Lambda}$ if the probability was greater than 0.70 and greater than that of the K_s^0 fit. These criteria are biased toward minimizing the contamination of the $\bar{\Lambda}$ sample. In events with two or more V^0's, strangeness conservation rules were invoked to resolve ambiguities whenever possible. After these assignments, there were no 3-way $K_s^0/\Lambda/\bar{\Lambda}$ ambiguities, and only one $\Lambda/\bar{\Lambda}$ ambiguity, which was resolved as a Λ on the basis of the χ^2 probability. The effectiveness of the selection procedure and the normalization corrections are discussed below. If the ambiguous decays had been resolved randomly, we would expect a 2.5 percent contamination of the resolved K_s^0 sample, a 3.4 percent contamination of the Λ sample, and a 20 percent contamination of the $\bar{\Lambda}$ sample. With ambiguities resolved using the χ^2 probability cuts, the actual contaminations are expected to be significantly less; however, these estimates can be taken as upper limits. Our procedure for resolving the ambiguous V^0's is admittedly somewhat arbitrary. Various other (generally more complex) procedures were also tried, but these caused no significant changes in the results.

The neutral V's that gave no fits could usually be understood in terms of multiple scattering or other effects that caused the attempted fits to be outside the probability cuts. An examination of these V's indicated that they were generally associated correctly with the primary interaction, and in many cases could be uniquely identified by a selection based on the invariant masses, assuming each of the four hypotheses above. By examining the invariant mass distributions, we estimate that this no-fit subsample contains 292 ± 112 K_s^0's, 118 ± 88 Λ's, and 10 ± 10 $\bar{\Lambda}$'s. Approximately 1 percent of the observed V^0 decays were incompatible with the four hypotheses above, but these are consistent with the expected number of unobserved scatters and three-body K_L^0 decays. The 11 percent subsample of neutral V's without 3C fits was not used in

computing the inclusive distributions that follow, because of the uncertainty in the momentum vectors. They were used, however, in normalizing these distributions, and in computing the cross sections.

Figs. 2(a)-(c) show the invariant mass distributions of all neutral V's, using $(\pi^+\pi^-)$, $(p\pi^-)$, and $(\bar{p}\,\pi^+)$ mass assignments corresponding to the K^0_s, Λ, and $\bar{\Lambda}$ decays, respectively. Note that in these figures, the invariant masses have been calculated from the observed track momenta before the 3C fits were attempted. In each figure, the unshaded area corresponds to the decays that were subsequently unambiguously identified by 3C fits, the diagonally hatched area corresponds to those that were resolved from the ambiguous decays, and the shaded area corresponds to the background of other V^0's (including γ conversions). The unfitted K^0_s, Λ, and $\bar{\Lambda}$ distributions peak at 0.498, 1.116, and 1.116 GeV/c^2 with full widths at half maximum of 8, 3, and 4 MeV/c^2, respectively. The error on the mean is less than 1 MeV/c^2 in each case. The results of the V^0 selections are summarized in Table I.

The validity of our selection criteria is demonstrated by the cos θ^+_D distributions in Figs. 2(d)-(f). Here θ^+_D is defined as the angle between the positive decay track and the direction of flight of the V^0 in the V^0 rest frame. The dips observed in the unambiguous (unshaded) portions are filled by the resolved ambiguous events, resulting in flat distributions as expected. We have examined distributions of the transverse momentum of the positive decay product with respect to the V^0 direction, and also V^0 invariant mass distributions using all combinations of incorrect mass assignments for the decay products; e.g. the $(\pi^+\pi^-)$ invariant mass spectrum for all V^0's identified as Λ's. In all cases, these distributions were smooth, with dips in the unambiguous portions being filled by the resolved ambiguous decays, and with no enhancements indicative of biased selections. As an additional check, we note that the number of K^0_s/Λ ambiguities resolved as K^0_s's is 100, while the number of $K^0_s/\bar{\Lambda}$ ambiguities

resolved as K_s^0's is 126. If all ambiguities could be resolved perfectly, we would expect these numbers to be equal because of the charge symmetry of the K_s^0 decay. The difference seen here is due to the assymetry in our procedure which favors Λ's over K_s^0's on one hand, but favors K_s^0's over $\bar{\Lambda}$'s on the other. Nevertheless, the closeness of these numbers supports the validity of our selection procedure.

To correct for unobserved strange particles that decay outside the fiducial volume or inside the 2.0 mm minimum length cut, a weight was calculated for each observed decay, based on the momentum of the particle and the potential path length from the primary interaction vertex to the boundary of the secondary fiducial volume. The averages of these weights are listed in Table I. Except for Fig. 2, all figures and tables have been corrected with these weights.

We have examined the invariant decay length ($c\tau$) distributions for each type of neutral strange particle and determined the corrected mean values in order to check the detection and identification efficiencies and to check the fiducial cuts. Using a maximum likelihood method, we have measured the average lifetimes (expressed in terms of the average invariant decay lengths) to be 2.69 ± 0.06 cm, 7.61 ± 0.22 cm, and 8.19 ± 1.72 cm for the K_s^0, Λ, and $\bar{\Lambda}$, respectively. The established[27] mean values of $c\tau$ are 2.675 cm for the K_s^0 and 7.89 cm for the Λ and $\bar{\Lambda}$. The values we measure indicate that our V^0 identification procedure is satisfactory, and that we have no significant fiducial biases. Without a minimum length cut, the losses below 2.0 mm would correspond to 2 percent of all V^0's. The short-distance losses beyond 2.0 mm are negligible.

3. Total and Topological Cross Sections

The total and topological cross sections are listed in Table II for events with K_s^0, Λ, or $\bar{\Lambda}$ particles. These cross sections were measured by counting the V^0's above back-

ground in the unfitted mass distributions of Figs. 2(a)-(c) and normalizing to the total corrected number of hadronic events. Corrections were made for branching ratios to unobserved decay modes and for escape probabilities. Because of particular experimental difficulties associated with 11-prong events, the K_s^0 cross section reported for this topology is based on a subset of data for which the 11-prong efficiency is well understood. It should be noted that cross sections reported in this paper include indirect sources, such as K_s^0's from K^* decays, and Λ's from Σ^0 decays.

We observe that the K_s^0 photoproduction cross section is approximately 1.7 times larger than that of Λ production, and that the $\bar{\Lambda}$ cross section is about 6% of the Λ cross section. These ratios are consistent with those obtained by averaging the measurements from $\pi^+ p$ and $\pi^- p$ interactions[1] at 18.5 GeV/c, a beam momentum close to that of this experiment. However, the actual numbers of K_s^0's, Λ's, and $\bar{\Lambda}$'s per inelastic event we have measured are all about 20 percent higher than the averages from the $\pi^+ p$ and $\pi^- p$ experiments. This suggests that the photon interacts much like a combination of π^+ and π^- mesons, but with an extra proclivity for strange particle production due to the direct coupling of the photon to $s\bar{s}$ quark pairs.

Figure 3 shows the average numbers of K_s^0's, Λ's, and $\bar{\Lambda}$'s per inelastic event, as a function of the available energy, compared to measurements from several πp fixed-target experiments[1,3,4,5,8]. The available energy, E_A, is defined as the total center-of-mass energy of the collision, minus the masses of the initial state particles. We observe that the numbers of neutral strange particles per event from the various fixed-target experiments all fall approximately on the same curves when plotted against this variable. This behavior has been reported previously for the total charged multiplicity in various experiments[28]. The solid lines in Fig. 3 were fitted by eye to the $\pi^- p$ fixed-target data. The dashed curve is a parametrization of the total charged multiplicity from Ref. 28, divided by 50. K_s^0 production is seen to rise with energy with roughly

the same slope as the total charged multiplicity, and noticably more steeply than Λ production. This suggests that K_s^0's are produced by some fragmentation process along with other particles and thus have the same energy dependence, while Λ's, on the other hand, are associated mainly with target excitations, and therefore not strongly energy-dependent beyond the threshold region. This hypothesis is further supported by the observation that Λ's are produced primarily in the backward hemisphere, as shown in the next section.

Also included in Fig. 3 are data points from e^+e^- annihilation experiments[17,18,19]. The e^+e^- points follow a trend which is similar to that for the fixed target experiments. K_s^0 production, however, is consistently higher by a large factor in the e^+e^- experiments than in the fixed-target experiments. The e^+e^- experiments typically report the sum of $\Lambda + \bar{\Lambda}$ production together, since they are symmetric in e^+e^- annihilation, in contrast to fixed-target experiments, which contain a baryon in the initial state. To make a meaningful comparison, we have divided the $(\Lambda + \bar{\Lambda})$ measurements in half to get the $\bar{\Lambda}$ (or Λ) fractions alone, and plotted them with the other points. It is interesting to note that these values lie above the fixed-target $\bar{\Lambda}$ points by a factor that is about the same as that noted for K_s^0 production, and that the slope is also similar to that of the fixed target experiments.

Included in Table II are the average multiplicities and dispersions of directly-produced charged particles in K_s^0, Λ, and $\bar{\Lambda}$ events. We observe that the multiplicities of events with K_s^0's and Λ's are approximately equal, and that they are lower by about a half unit than the average multiplicity of all hadronic events (observed to be 4.40 ± 0.10). Events with visible $\bar{\Lambda}$'s have still lower average multiplicity. This may be simply a kinematic effect, since events containing a $\bar{\Lambda}$ must have at least two additional baryons in the final state; thus, nearly half the total center-of-mass energy is taken by these three masses (two of which are neutral in the simplest topology), leaving little

phase space left for extra charged particles. The multiplicity distributions for the three samples all peak at 3-prongs. The dispersions, $D = (\langle n^2 \rangle - \langle n \rangle^2)^{1/2}$, for all events, and for events with K_s^0's, Λ's, or $\bar{\Lambda}$'s, are all equal, within errors, despite the differences in their multiplicities.

4. Inclusive Distributions

In Table III, we present our invariant cross section measurements

$$F(x) = \int \frac{2E^*}{\pi\sqrt{s}} \frac{d^2\sigma}{dx\, dp_T^2}\, dp_T^2$$

for inclusive production of K_s^0, Λ, and $\bar{\Lambda}$ particles as functions of the Feynman scaling variable x ($= 2p_L^*/\sqrt{s}$). Here E^* and p_L^* are the energy and longitudinal momentum of the produced particle in the overall center-of-mass system, and $\sqrt{s}$ is the total c.m.s. energy. These measurements, normalized to the total cross section σ_T, are plotted in Figs. 4(a)-(c). The K_s^0 and $\bar{\Lambda}$ distributions peak in the forward hemisphere at about $x \simeq 0.1$, suggesting a beam fragmentation mechanism, while the Λ's spread through the backward region, peaking at about -0.5. Data from several lepton[12,14,22] and hadron[1] beam experiments, normalized in each case to the total inelastic cross section appropriate for that process, are plotted in the same figures. The general agreement among the various processes in both the shape and absolute magnitude of the distributions for all three strange particle types suggests a similar production mechanism for these particles. We have no explanation for why the Λ photoproduction data from Ref. 22 are systematically below the other experiments, except to note that the authors of that paper estimate an overall normalization uncertainty of 30 to 40 percent. Except for the very forward region ($x > 0.5$), the similarity between our data and data from πp interactions[1] is particularly striking. As noted in the previous section, the strange particle production fractions in this experiment are about

20 percent higher than the averages from π^+p and π^-p experiments. As shown in Fig. 4, the γp points from this experiment are generally close to or slightly above the π^-p points, which in turn are above the π^+p points. The curves superimposed on the Λ and $\bar{\Lambda}$ data are taken from a diquark fusion model calculation by Donnachie[29]. The curves were calculated for an incident pion beam, and the normalization is arbitrary. Both curves follow the general trend of the data, but the Λ curve deviates significantly from the photoproduction data in the far forward and backward regions.

We have fitted our data with functions of the form $A(1-|x|)^\alpha$ over various restricted ranges of x to allow comparisons with the quark counting rules for leading hadron production as suggested by Gunion[30]. The results of the fits are shown by the solid lines in Fig. 5 and are listed in Table IV, along with the predicted values of α. In this model, the exponent α depends on the quark contents of both the target proton and the photon, which we treat like a meson, as well as on the details of the fragmentation process. The curves appear to describe the data reasonably well, even though the model treats only leading order effects and is expected to be strictly valid only in the limits of $x = \pm 1$. For Λ production, we see a qualitative agreement between the measured and predicted values of α. For both K^0_s and $\bar{\Lambda}$ production, the measured values fall more steeply than the predictions in the forward region, and less steeply in the backward region.

In Fig. 6, the z distributions of our data (Table V) are plotted along with data from various lepton scattering experiments[12,13,16,18]. The inclusive variable z, which is defined as the energy of the outgoing particle (in the lab frame) divided by the energy of the photon (or intermediate boson in the case of neutrino scattering), is similar to x but does not require a knowledge of the photon's direction, and thus can be used for comparisons with e^+e^- annihilation results. As in the x distributions, our photoproduction data for K^0_s's and Λ's are similar to data from other fixed target

experiments when plotted as a function of z. The $\bar{\Lambda}$ distributions from μp and e^+e^- interactions in Fig. 6(c) have been normalized to give the same total number of $\bar{\Lambda}$'s as seen in this experiment. Unlike the $\bar{\Lambda}$ distributions from those experiments, however, the distribution we measure peaks at about 0.2, which corresponds roughly to the γp center-of-mass.

The p_T^2 distributions for K_s^0, Λ and $\bar{\Lambda}$ production are shown in Fig. 7. The solid lines show the best fits of the form $ae^{-bp_T^2}$ to each of the distributions. The data are listed in Table VI, and the fitted parameters are given in Table VII. The slope parameters we observe at $p_T^2 \leq 1\ (GeV/c)^2$ are compatible with those measured in πN and pp interactions.[1-9] Our results can be compared with those for the K_s^0 and Λ data from a deep-inelastic electroproduction experiment[12] ($b_{K_s^0} = 4.3 \pm 0.5\ GeV^{-2}$ and $b_\Lambda = 4.2 \pm 0.3\ GeV^{-2}$) and from a $\bar{\nu} N$ experiment[14] ($b_{K_s^0} = 4.31 \pm 0.35\ GeV^{-2}$ and $b_\Lambda = 4.45 \pm 0.32\ GeV^{-2}$). In the p_T^2 distribution for K_s^0 production, there is a break in the slope at $p_T^2 \sim 0.3\ (GeV/c)^2$, below which the slope is steeper than those of the Λ and $\bar{\Lambda}$. A similar break has been observed for K_s^0 production in 16 GeV $\pi^+ p$ interactions[2], in 24 GeV $\pi^+ d$ interactions[10], and in 405 GeV pp interactions.[7]

5. Polarization of Λ and $\bar{\Lambda}$

Figure 8 shows the average polarization of the photoproduced Λ's as a function of x and of p_T. The polarization is given by

$$P = \frac{3}{\alpha} \left\langle \hat{p} \cdot \hat{n} \right\rangle \quad ,$$

where $\hat{p}$ is a unit vector in the direction of the decay proton in the rest frame of the Λ, and $\hat{n}$ is the normal to the production plane, defined by

$$\hat{n} = \frac{\hat{\gamma} \times \hat{v}}{|\hat{\gamma} \times \hat{v}|} \quad .$$

$\hat{\gamma}$ and $\hat{v}$ are unit vectors in the directions of the incident photon and the Λ, respectively. The weak decay asymmetry parameter, α, was taken[27] to be 0.642. We have found that the polarization measurement is sensitive to small inefficiencies near the edges of the fiducial volume and to contamination of the Λ sample by other particles; thus, we have repeated the polarization calculation with variations in the cuts, and in addition, we have applied the calculation procedure to the K_s^0 sample in order to estimate the systematic errors. With the same cuts used for the Λ polarization, we have measured the average polarization of the K_s^0's (which are spin-0 mesons and have no polarization axis) to be 0.01 ± 0.01. We use this as a basis for estimating the systematic error in the Λ sample.

The overall Λ polarization was observed to be 0.09 ± 0.07 where the error includes an estimate of the systematic uncertainty, but is dominated by statistics. Integrated over p_T, the Λ polarization is x-dependent, being positive in the backward hemisphere ($x < 0$) and negative in the forward hemisphere ($x > 0$). This is very similar to the x dependence seen in the $\pi^- p$ experiment[1] mentioned earlier, as shown in Fig. 8. A small net positive polarization was also observed in the CERN-Omega photoproduction experiment[22], but no x dependence was reported. The polarization of Λ's in the backward hemisphere increases with transverse momentum. Strong transverse momentum dependence of Λ polarization has been reported previously in hadronic interactions[5,10,11]. It should be noted that the production plane is undefined when $p_T = 0$; thus, the polarization must be zero in this limit.

The polarization picture for $\bar{\Lambda}$'s is less clear. While we see a net negative polarization of -0.4 ± 0.4 (taking $\alpha = -0.642$ in this case), consistent with the other photoproduction experiment[22], the low statistics make meaningful x and p_T dependent measurements of the polarization difficult.

6. Inclusive $K^*(890)$ and $\Sigma^*(1385)$ Production

The effective mass distributions for the $(K_s^0\pi^+)$ and $(K_s^0\pi^-)$ systems and their sum, weighted to correct for the K_s^0 escape probability, are shown in Figs. 9(a)-(c). We observe a clear $K^*(890)$ signal at $M(K^0\pi) \approx 890$ MeV with ~ 70 MeV width. To obtain the $K^*(890)$ production cross sections, we fitted each of these distributions with a function consisting of a background of the form aM^be^{-cM}, plus a Gaussian for the resonance, where a, b and c are the fitting parameters. The mass and width were taken to be $M_0 = 890$ MeV and $\sigma_0 = 30$ MeV, respectively. The fitted functions are illustrated by the solid lines in Figs. 9(a)-(c). After subtraction of the background, the fit results were corrected for the branching ratio to $K^\pm\pi^o$ and were multiplied by 2 to account for the unseen $K_L^0\pi^\pm$ decays. The production cross sections are as follows:

$$\sigma(K^{*+}(890)) = 3.27 \pm 0.35\ \mu b \quad ,$$

$$\sigma(K^{*-}(890)) = 1.90 \pm 0.28\ \mu b \quad ,$$

$$\sigma(K^{*\pm}(890)) = 5.14 \pm 0.46\ \mu b \quad .$$

The production of $\Sigma^*(1385)$ baryons and their decays via the $\Lambda\pi$ channel were analyzed in the same way as for the $K^*(890)$. In this case, the $\Lambda\pi^+$, $\Lambda\pi^-$, and $\Lambda\pi^\pm$ distributions were fitted with functions of the same form, with the mass and width of the gaussian taken to be $M_0 = 1380$ MeV and $\sigma = 30$ MeV, respectively. The weighted $\Lambda\pi$ mass distributions are shown in Figs. 10(a)-(c), along with the fitted functions. The $\Sigma^*(1385)$ production cross sections, corrected for the decay branching ratio, are as follows:

$$\sigma(\Sigma^{*+}(1385)) = 0.60 \pm 0.10\ \mu b \quad ,$$

$$\sigma(\Sigma^{*-}(1385)) = 0.36 \pm 0.08\ \mu b \quad ,$$

$$\sigma(\Sigma^{*\pm}(1385)) = 0.94 \pm 0.13\ \mu b \quad .$$

To facilitate comparisons with other experiments, the ratios $\sigma(K^*(890))/\sigma(K^0_s)$ and $\sigma(\Sigma^*(1385))/\sigma(\Lambda)$, corrected for branching ratios, are listed in Table VIII. The errors on the cross sections and ratios reported in this section are statistical only. Systematic errors related to the chosen form of the background function and resonance shape dominate the overall normalization. We estimate a systematic uncertainty of ± 15 percent for the K^{*+} and Σ^{*+}, and ± 30 percent for the K^{*-} and Σ^{*-}. Our ratio $\sigma(K^{*+})/\sigma(K^0_s) = 0.35 \pm 0.04$ is close to the value of 0.30 ± 0.06 measured in a $\pi^- p$ experiment[5] at 15 GeV/c, but lower than that of 0.55 ± 0.14 obtained in pp interactions[7] at a much higher energy. Various theoretical models also predict higher ratios than those we observe. An additive quark model[31] predicts equal $\sigma(K^{*+})/\sigma(K^0)$ and $\sigma(K^{*-})/\sigma(K^0)$ ratios of 0.7 in the central region (defined as $|x| < 1/3$), increasing to 0.75 in the photon fragmentation region ($1/2 < x < 3/4$). Here we have taken the strange quark suppression factor, λ, to be 0.3 as suggested by the authors of Ref. 31. In the multiperipheral resonance production model[32], the ratios are predicted to be $\sigma(K^*)/\sigma(K^0) = 0.53 - 0.62$. Our data indicate a substantially lower production rate. It should be noted that these models assume an energy regime in which K^0 and $\bar{K}^0$ production are equal, in which case the denominators, $\sigma(K^0_s)$ and $\sigma(K^0)$, would be the same. This assumption is clearly not valid at our energy. For example, we observe that $\sigma(K^{*+})$ is larger than $\sigma(K^{*-})$ by a factor of 1.7. This difference can be understood as a consequence of strangeness conservation, if much of the strange meson cross section [$\sigma(K^{*+})$, but not $\sigma(K^{*-})$] is associated with production of strange Λ or Σ baryons.

We have measured the $\sigma(\Sigma^{*+})/\sigma(\Lambda)$ and $\sigma(\Sigma^{*-})/\sigma(\Lambda)$ ratios to be 0.11 ± 0.02 and 0.06 ± 0.02, respectively. The $\sigma(\Sigma^{*-})/\sigma(\Lambda)$ value is equal or very close to values measured in pp experiments[6,7,9] over a wide energy range, but the $\sigma(\Sigma^{*+})/\sigma(\Lambda)$ measurement is smaller than those of the pp experiments by factor of 2/3. While part of this difference might be accounted for by the presence of two baryons in the initial state

of the pp interactions, compared to only one in this experiment, a significant difference also exists between our measurement and the $\pi^- p$ experiment[5]. The additive quark model mentioned above predicts $\sigma(\Sigma^{*+})/\sigma(\Lambda)$ and $\sigma(\Sigma^{*-})/\sigma(\Lambda)$ ratios of 0.25 for the central region (independent of the charge of the Σ^*), and 0.28 and 0.13, respectively, for the photon fragmentation region. These predictions are significantly higher than the observations.

7. Conclusion

We have performed a high-statistics bubble chamber study of neutral strange particles produced in 20 GeV γp interactions. We have examined various features of the final states of these interactions and compared them with other strange particle production processes involving beams of electrons, neutrinos, and hadrons over a wide energy range. The similarities are striking, indicating that a common underlying mechanism is responsible for the development of the final states in these various processes. The longitudinal and transverse momentum distributions of K_s^0, Λ, and $\bar{\Lambda}$ particles, and the polarization of the Λ's measured in this experiment are remarkably similar, in both shape and normalization, to those measured in a $\pi^- p$ experiment[1] near this energy. The fractional production cross sections are about 20 percent higher than the averages of these fractions measured in $\pi^+ p$ and $\pi^- p$ interactions. This suggests that the incident photon is much like a meson with an enhanced probability for producing strange particles.

We wish to thank the SLAC bubble chamber crew for their tireless dedication. We gratefully acknowledge the efforts of the film scanning and measuring personnel at the participating institutions.

This work was supported by the Japan-U.S. Cooperative Research Project on High Energy Physics under the Japanese Ministry of Education, Science and Culture; the

U.S. Department of Energy; the Science and Engineering Research Council (U.K.); the U.S. National Science Foundation; the U.S.-Israel Binational Science Foundation; and the Israel Academy of Sciences Commission for Basic Research.

REFERENCES

* Work supported by the Department of Energy, contract DE-AC03-76SF00515.

† Max Kade Foundation Fellow.

‡ Present address: Technology for Communication International, Mountain View, California, USA.

§ On leave from Technion-Israel Institute of Technology, Haifa, Israel.

¶ Present address: University of Tokyo, Tokyo, Japan.

1. P. H. Stuntebeck et al., Phys. Rev. D 9, 608 (1974).
2. P. Bosetti et al., Nucl. Phys. B94, 21 (1975).
3. D. Ljung et al., Phys. Rev. D 15, 3l63 (1977).
4. D. Bogert et al., Phys. Rev. D 16, 2098 (1977).
5. F. Barreiro et al., Phys. Rev. D 17, 669 (1978).
6. V. Blobel et al., Nucl. Phys. B69, 454 (1974); Phys. Lett. 48B, 73 (1974); K. Böckmann et al., Nucl. Phys. B143, 395 (1978).
7. H. Kichimi et al., Phys. Rev. D 20, 37 (1979).
8. R. Sugahara et al., Nucl. Phys. B156, 237 (1979).
9. F. LoPinto et al., Phys. Rev. D 22, 573 (1980).
10. S. Dado et al., Phys. Rev. D 22, 2656 (l980).
11. K. Raychaudhuri et al., Phys. Lett. 90B, 319 (1980).
12. I. Cohen et al., Phys. Rev. Lett. 40, 1614 (1978).
13. R. G. Hicks, et al., Phys. Rev. Lett. 45, 765 (1980).
14. V. Ammosov et al., Nucl. Phys. B162, 205 (1980).
15. V. V. Ammosov et al., Nucl. Phys. B177, 365 (1981).
16. H. Grässler et al., Nucl. Phys. B194, 1 (1982).
17. V. Lüth et al., Phys. Lett. 70B, 120 (1977).

18. R. Brandelik et al., Phys. Lett. 105B, 75 (1981).

19. CLEO Collaboration, contribution to the XXI International Conference on High Energy Physics, Paris, July, 1982; CLNS 82/547.

20. R. Erbe et al., Phys. Rev. 188, 2060 (1969).

21. H. H. Bingham et al., Phys. Rev. D 8, 1277 (1973).

22. D. Aston et al., Nucl. Phys. B195, 189 (1982).

23. J. E. Brau et al., Nucl. Instrum. Methods 196, 403 (1982).

24. A. Bevan et al., Nucl. Instrum. Methods 203, 159 (1982).

25. D. O. Caldwell et al., Phys. Rev. Lett. 40, 1222 (1978).

26. In this experiment, the three main cameras were supplemented by a special high-resolution camera, with which we could detect secondary decays as close as 0.3 mm from the primary interaction vertex. This fourth camera was developed for the study of charmed particles and could, in principle, be used to identify most of the neutral strange particle decays inside the 2.0 mm cut. However, we have not used the extra information gained with this camera for the analysis presented here.

27. Particle Data Group, Phys. Lett. 111B, (1982).

28. D. Haidt, Proceedings of the 10th International Symposium on Lepton and Photon Interactions at High Energies, Bonn, 1981, p. 558.

29. A. Donnachie, Z. Physik C, Particles and Fields 4, 161-167 (1980).

30. J. F. Gunion, Phys. Lett. 88B, 150 (1979).

31. V. V. Anisovich and V. M. Shekhter, Nucl. Phys. B55, 455 (1973).

32. M. Fukugita et al., Phys. Rev. D 19, 187 (1979).

33. D. Aston et al., Nucl. Phys. B198, 189 (1982).

Table I

Identification statistics for kinematically fitted V^0's after the removal of $\gamma \rightarrow e^+e^-$ conversions, as described in the text. There were no 3-way $K^0/\Lambda/\bar{\Lambda}$ ambiguities. The weights listed here are corrections for the escape probabilities.

	Observed V's	Weighted V's	Average Weight
Unique K_s^0	4070	4912	1.207
Unique Λ	2005	2372	1.183
Unique $\bar{\Lambda}$	91	127	1.396
Ambiguous K_s^0/Λ	549		
Ambiguous $K_s^0/\bar{\Lambda}$	155		
Ambiguous $\Lambda/\bar{\Lambda}$	1		
Resolved K_s^0	4296	5196	1.210
Resolved Λ	2455	2949	1.201
Resolved $\bar{\Lambda}$	120	167	1.394

Table II

K^0_s, Λ, and $\bar{\Lambda}$ production cross sections,
corrected for neutral decay modes.

n_{ch} (number of charged prongs)	$\sigma(nb)$ K^0_s	Λ	$\bar{\Lambda}$
1	1011 ± 57	737 ± 50	72 ± 15
3	4109 ± 155	2533 ± 123	75 ± 26
5	3150 ± 125	1734 ± 92	62 ± 13
7	1010 ± 55	530 ± 41	21 ± 7
9	132 ± 17	73 ± 13	
11	34 ± 16		
Total inclusive	9447 ± 318	5600 ± 244	329 ± 40
$\langle n_{ch} \rangle$	3.99 ± 0.03	3.82 ± 0.04	3.20 ± 0.15
$D = (\langle n^2_{ch} \rangle - \langle n_{ch} \rangle^2)^{1/2}$	1.79 ± 0.09	1.76 ± 0.12	1.62 ± 0.45

Table III

x dependence of the K_s^0, Λ and $\bar{\Lambda}$ production cross sections, corrected for neutral decay modes.

K_s^0		Λ		$\bar{\Lambda}$	
x Range	$\frac{2E^*}{\pi\sqrt{s}}\frac{d\sigma}{dx}$ (μb)	x Range	$\frac{2E^*}{\pi\sqrt{s}}\frac{d\sigma}{dx}$ (μb)	x Range	$\frac{2E^*}{\pi\sqrt{s}}\frac{d\sigma}{dx}$ (μb)
−0.7 to −0.6	$3.5 \pm 1.1 \times 10^{-2}$	−1.0 to −0.9	$18.9 \pm 4.4 \times 10^{-2}$	−1.0 to −0.7	$0.57 \pm 0.33 \times 10^{-2}$
−0.6 to −0.5	$10.4 \pm 2.6 \times 10^{-2}$	−0.9 to −0.8	$74.2 \pm 8.0 \times 10^{-2}$	−0.7 to −0.4	$0.82 \pm 0.34 \times 10^{-2}$
−0.5 to −0.4	$16.0 \pm 3.7 \times 10^{-2}$	−0.8 to −0.7	$112.8 \pm 9.2 \times 10^{-2}$	−0.4 to −0.2	$1.18 \pm 0.46 \times 10^{-2}$
−0.4 to −0.3	$30.1 \pm 4.8 \times 10^{-2}$	−0.7 to −0.6	$123.8 \pm 9.0 \times 10^{-2}$	−0.2 to −0.1	$4.37 \pm 1.22 \times 10^{-2}$
−0.3 to −0.2	$56.1 \pm 7.9 \times 10^{-2}$	−0.6 to −0.5	$127.4 \pm 9.9 \times 10^{-2}$	−0.1 to 0.0	$8.86 \pm 1.79 \times 10^{-2}$
−0.2 to −0.1	$71.0 \pm 4.4 \times 10^{-2}$	−0.5 to −0.4	$116.3 \pm 9.1 \times 10^{-2}$	0.0 to 0.1	$9.73 \pm 1.99 \times 10^{-2}$
−0.1 to 0.0	$100.8 \pm 5.5 \times 10^{-2}$	−0.4 to −0.3	$110.1 \pm 8.5 \times 10^{-2}$	0.1 to 0.2	$7.48 \pm 1.86 \times 10^{-2}$
0.0 to 0.1	$134.1 \pm 6.9 \times 10^{-2}$	−0.3 to −0.2	$85.0 \pm 6.2 \times 10^{-2}$	0.2 to 0.3	$5.94 \pm 1.93 \times 10^{-2}$
0.1 to 0.2	$142.0 \pm 7.7 \times 10^{-2}$	−0.2 to −0.1	$78.0 \pm 5.8 \times 10^{-2}$	0.3 to 0.45	$1.77 \pm 0.80 \times 10^{-2}$
0.2 to 0.3	$121.2 \pm 7.5 \times 10^{-2}$	−0.1 to 0.0	$60.4 \pm 4.9 \times 10^{-2}$	0.45 to 0.60	$0.90 \pm 0.90 \times 10^{-2}$
0.3 to 0.4	$84.5 \pm 6.5 \times 10^{-2}$	0.0 to 0.1	$39.1 \pm 3.9 \times 10^{-2}$		
0.4 to 0.5	$57.3 \pm 5.8 \times 10^{-2}$	0.1 to 0.2	$33.4 \pm 3.9 \times 10^{-2}$		
0.5 to 0.6	$39.7 \pm 5.4 \times 10^{-2}$	0.2 to 0.3	$27.3 \pm 3.9 \times 10^{-2}$		
0.6 to 0.7	$19.2 \pm 4.1 \times 10^{-2}$	0.3 to 0.4	$17.4 \pm 3.3 \times 10^{-2}$		
0.7 to 0.8	$5.6 \pm 2.3 \times 10^{-2}$	0.4 to 0.5	$8.4 \pm 2.6 \times 10^{-2}$		
0.8 to 0.9	$1.0 \pm 1.0 \times 10^{-2}$	0.5 to 0.6	$4.9 \pm 2.0 \times 10^{-2}$		

Table IV

The parameter α in the function $F(x) = A(1 - |x|)^{\alpha}$ fitted to the K_s^0, Λ, and $\bar{\Lambda}$ distributions of Fig. 5, along with values predicted by quark counting rules as explained in the text.

Reaction	Range of x	Fitted α	Predicted α	χ^2/DF
$\gamma p \to K_s^0 X$	$-0.7 < x < 0$	3.29 ± 0.17	4	5.1/5
	$0.3 < x < 0.9$	2.50 ± 0.24	1	2.5/4
$\gamma p \to \Lambda + X$	$-1 < x < -0.5$	0.90 ± 0.06	1	6.1/2
	$0.1 < x < 0.6$	2.95 ± 0.47	2	1.3/3
$\gamma p \to \bar{\Lambda} + X$	$-0.7 < x < 0$	3.48 ± 0.34	5	6.0/2
	$0.1 < x < 0.6$	4.09 ± 1.28	2	0.8/2

Table V

z dependence of the K^0_s, Λ and $\bar{\Lambda}$ production cross sections, corrected for neutral decay modes.

K^0_s		Λ		$\bar{\Lambda}$	
z Range	$\frac{1}{\sigma_T}\frac{d\sigma}{dz}$	z Range	$\frac{1}{\sigma_T}\frac{d\sigma}{dz}$	z Range	$\frac{1}{\sigma_T}\frac{d\sigma}{dz}$
0.025 to 0.05	$317.8 \pm 27.7 \times 10^{-3}$	0.05 to 0.10	$435.4 \pm 23.1 \times 10^{-3}$	0.05 to 0.10	$3.98 \pm 1.24 \times 10^{-3}$
0.05 to 0.10	$343.2 \pm 27.0 \times 10^{-3}$	0.10 to 0.15	$244.2 \pm 13.5 \times 10^{-3}$	0.10 to 0.20	$9.09 \pm 1.53 \times 10^{-3}$
0.10 to 0.15	$281.9 \pm 14.9 \times 10^{-3}$	0.15 to 0.20	$109.3 \pm 7.9 \times 10^{-3}$	0.20 to 0.30	$10.03 \pm 1.77 \times 10^{-3}$
0.15 to 0.20	$224.1 \pm 12.8 \times 10^{-3}$	0.20 to 0.25	$65.3 \pm 6.0 \times 10^{-3}$	0.30 to 0.40	$4.72 \pm 1.20 \times 10^{-3}$
0.20 to 0.25	$168.2 \pm 10.6 \times 10^{-3}$	0.25 to 0.30	$32.2 \pm 4.1 \times 10^{-3}$	0.40 to 0.50	$1.85 \pm 0.77 \times 10^{-3}$
0.25 to 0.30	$127.2 \pm 10.2 \times 10^{-3}$	0.30 to 0.35	$26.2 \pm 3.8 \times 10^{-3}$	0.50 to 0.70	$0.38 \pm 0.27 \times 10^{-3}$
0.30 to 0.35	$97.7 \pm 7.6 \times 10^{-3}$	0.35 to 0.40	$22.1 \pm 3.8 \times 10^{-3}$		
0.35 to 0.40	$70.7 \pm 6.6 \times 10^{-3}$	0.40 to 0.45	$13.8 \pm 3.0 \times 10^{-3}$		
0.40 to 0.45	$50.4 \pm 5.3 \times 10^{-3}$	0.45 to 0.55	$6.53 \pm 1.48 \times 10^{-3}$		
0.45 to 0.55	$31.0 \pm 3.2 \times 10^{-3}$	0.55 to 0.70	$2.43 \pm 0.68 \times 10^{-3}$		
0.55 to 0.65	$15.5 \pm 2.3 \times 10^{-3}$				
0.65 to 0.75	$6.21 \pm 2.10 \times 10^{-3}$				
0.75 to 0.90	$1.65 \pm 0.65 \times 10^{-3}$				

Table VI

p_T^2 dependence of the K_s^0, Λ and $\bar{\Lambda}$ production cross sections, corrected for neutral decay modes.

K_s^0		Λ		$\bar{\Lambda}$	
p_T^2 Range $(GeV/c)^2$	$d\sigma/dp_T^2$ $[\mu b/(GeV/c)^2]$	p_T^2 Range $(GeV/c)^2$	$d\sigma/dp_T^2$ $[\mu b/(GeV/c)^2]$	p_T^2 Range $(GeV/c)^2$	$d\sigma/dp_T^2$ $[\mu b/(GeV/c)^2]$
0.00 to 0.05	43.35 ± 2.20	0.00 to 0.05	18.44 ± 1.13	0.0 to 0.1	1.08 ± 0.18
0.05 to 0.10	31.18 ± 1.70	0.05 to 0.10	14.32 ± 0.95	0.1 to 0.2	0.705 ± 0.149
0.10 to 0.15	22.26 ± 1.32	0.10 to 0.15	11.37 ± 0.82	0.2 to 0.3	0.530 ± 0.129
0.15 to 0.20	17.97 ± 1.14	0.15 to 0.20	10.76 ± 0.81	0.3 to 0.4	0.418 ± 0.116
0.20 to 0.25	13.66 ± 0.94	0.20 to 0.25	8.34 ± 0.68	0.4 to 0.6	0.128 ± 0.044
0.25 to 0.30	9.80 ± 0.76	0.25 to 0.30	6.69 ± 0.60	0.6 to 0.8	0.052 ± 0.027
0.30 to 0.35	9.17 ± 0.74	0.30 to 0.40	5.81 ± 0.42	0.8 to 1.0	0.054 ± 0.031
0.35 to 0.40	6.50 ± 0.59	0.40 to 0.50	3.74 ± 0.32		
0.40 to 0.45	4.85 ± 0.52	0.50 to 0.60	2.73 ± 0.28		
0.45 to 0.55	4.21 ± 0.36	0.60 to 0.70	1.91 ± 0.22		
0.55 to 0.65	2.79 ± 0.28	0.70 to 0.85	1.47 ± 0.17		
0.65 to 0.75	1.77 ± 0.21	0.85 to 1.00	0.628 ± 0.101		
0.75 to 0.85	1.29 ± 0.16	1.10 to 1.15	0.677 ± 0.131		
0.85 to 0.95	0.945 ± 0.163	1.15 to 1.30	0.332 ± 0.079		
0.95 to 1.05	0.488 ± 0.106	1.30 to 1.50	0.259 ± 0.060		
1.05 to 1.15	0.411 ± 0.104	1.50 to 1.75	0.072 ± 0.037		
1.15 to 1.35	0.180 ± 0.078				
1.35 to 1.55	0.117 ± 0.037				
1.55 to 1.80	0.060 ± 0.023				

Table VII

The parameters a and b of the function $d\sigma/dp_T^2 = ae^{-bp_T^2}$ fitted to the p_T^2 distributions of K_s^0, Λ, and $\bar{\Lambda}$ particles.

Reaction	Range of p_T^2 $(GeV/c)^2$	a $\mu b/(GeV/c)^2$	b $(GeV/c)^{-2}$	χ^2/DF
$\gamma p \to K_s^0 + X$	$0 < p_T^2 < 0.3$	50.2 ± 3.6	5.8 ± 0.5	0.5/4
	$0.3 < p_T^2 < 1.8$	30.4 ± 5.0	4.0 ± 0.3	2.4/11
$\gamma p \to \Lambda + X$	$0 < p_T^2 < 1.75$	19.3 ± 1.3	3.3 ± 0.2	4.3/11
	$0 < p_T^2 < 1.0$	18.5 ± 1.4	3.6 ± 0.2	1.9/10
$\gamma p \to \bar{\Lambda} + X$	$0 < p_T^2 < 1.0$	1.4 ± 0.4	4.0 ± 1.0	0.8/5

Table VIII

Ratios of $K^*(890)$ and $\Sigma^*(1385)$ cross section to K^0_s and Λ cross sections in γp, πp, pp, νp and $\bar{\nu} N$ interactions.

Interaction		K^{*+}/K^0_s	K^{*-}/K^0_s	$K^{*\pm}/K^0_s$	Σ^{*+}/Λ	Σ^{*-}/Λ	$\Sigma^{*\pm}/\Lambda$
This exp.		0.35 ± 0.04	0.20 ± 0.03	0.54 ± 0.05	0.11 ± 0.02	0.06 ± 0.02	0.17 ± 0.03
15 GeV/c	$\pi^- p$ [a]	0.30 ± 0.06	...	...	0.16 ± 0.02	...	...
12	pp [b]	0.43 ± 0.05	0.03 ± 0.03	...	0.18 ± 0.02	0.06 ± 0.01	...
24	pp [b]	0.51 ± 0.05	0.11 ± 0.02	...	0.16 ± 0.02	0.07 ± 0.01	...
300	pp [c]	...	...	0.64 ± 0.22	...	...	0.15 ± 0.11
405	pp [d]	0.55 ± 0.14	0.48 ± 0.14	...	0.17 ± 0.03	0.11 ± 0.02	...
	νp [e]	0.63 ± 0.23	...	...	0.31 ± 0.09	...	...
	$\bar{\nu} N$ [f]	...	0.15 ± 0.06	...	...	0.05 ± 0.03	...
20 - 70	γp [g]	...	...	...	0.10 ± 0.02	0.07 ± 0.02	...

[a] Ref. 5. [b] Ref. 6. [c] Ref. 9. [d] Ref. 7. [e] Ref. 16. [f] Ref. 15. [g] Ref. 33.

FIGURE CAPTIONS

1. The SLAC Hybrid Facility as implemented for the 20 GeV γp experiment.
2. Invariant mass distributions of (a) $\pi^+\pi^-$, (b) $p\pi^-$, and (c) $\bar{p}\,\pi^+$ for V^0's identified as K^0_s, Λ, and $\bar{\Lambda}$ decays, respectively, along with distributions (d), (e), (f) of cos θ^+_D, where θ^+_D is the angle of the positive decay product with respect to the direction of the V^0 in the V^0 rest frame.
3. The average numbers of K^0_s's, Λ's and $\bar{\Lambda}$'s per event are plotted as a function of the available energy, E_A, defined as the total c.m.s. energy minus the masses of the initial state particles. Also plotted are results from other experiments (Refs. 1 [18.5 GeV/c $\pi^{\pm}p$]; 3 [205 GeV/c π^-p]; 4 [250 GeV/c π^-p]; 5 [15 GeV/c π^-p]; 8 [6 GeV/c π^-p]; 17 [1.8 $\times$ 1.8 and 2.6 $\times$ 2.6 GeV e^+e^-]; 18 [16 $\times$ 16 GeV e^+e^-]; 19 [5.2 $\times$ 5.2 GeV e^+e^-]). The dashed curve is a parametrization of the total charged multiplicity (Ref. 28), divided by 50. The solid lines were drawn to guide the eye.
4. Distributions of the invariant differential cross sections for (a) K^0_s, (b) Λ, and (c) $\bar{\Lambda}$ production in various processes (Refs. 1 [18.5 GeV/c $\pi^{\pm}p$]; 12 [11.5 GeV/c e^-p]; 14 [$\bar{\nu}_\mu N$]; 22 [25-34 GeV γp]) plotted as a function of the longitudinal momentum variable x. The data for each process are normalized to the corresponding total inelastic cross section σ_T. The curves illustrate a diquark fusion model calculation (Ref. 29).
5. The x-dependences of K^0_s, Λ, and $\bar{\Lambda}$ production. The solid lines represent fits of the form $A(1-|x|)^\alpha$; the dashed connecting lines were drawn by hand to guide the eye.

6. Fractional production cross sections for neutral strange particles as a function of z ($= E_{had}/E_{\gamma}$). Data shown here from other lepton scattering experiments (Refs. 12, 13, 16, 18) have been arbitrarily normalized to the same total number of strange particles.

7. Transverse momentum distributions for K_s^0, Λ, and $\bar{\Lambda}$ production. The solid lines represent fits of the form $ae^{-bp_T^2}$. The fit parameters are given in Table IV.

8. Average polarization of Λ's as a function of x and p_T. The open square points are from Ref. 1.

9. Invariant mass distributions for (a) $K^0\pi^+$, (b) $K^0\pi^-$, and (c) $K^0\pi^{\pm}$ combined. The curves represent the fits described in the text.

10. Invariant mass distributions for (a) $\Lambda\pi^+$, (b) $\Lambda\pi^-$, and (c) $\Lambda\pi^{\pm}$ combined. The curves represent the fits described in the text.

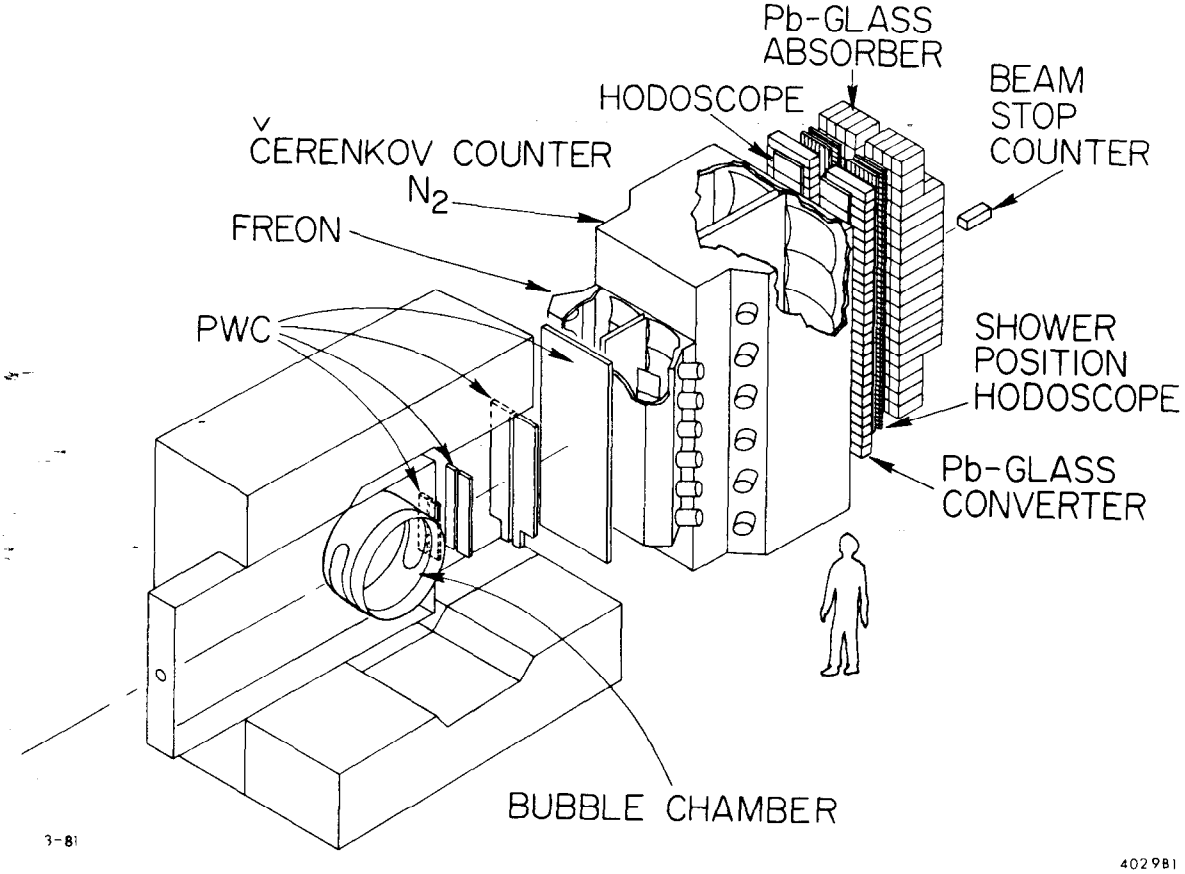
Pb-GLASS
ABSORBER
HODOSCOPE
BEAM
STOP
COUNTER
CERENKOV COUNTER
N_2
FREON
PWC
SHOWER
POSITION
HODOSCOPE
Pb-GLASS
CONVERTER
BUBBLE CHAMBER
3-81
4029B1

Fig. 1

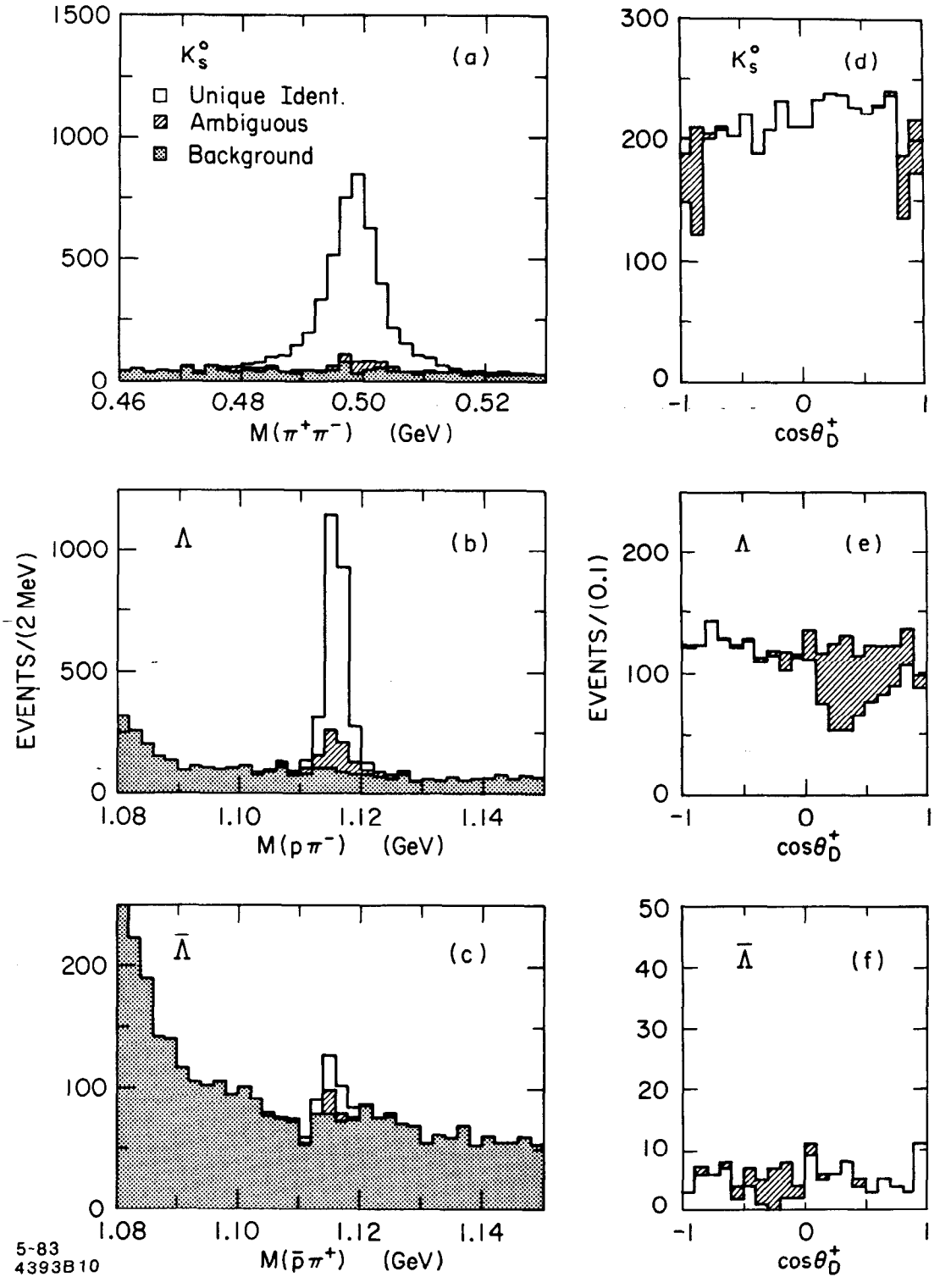
K_s°
(a)
Unique Ident.
Ambiguous
Background
1500
1000
500
0
0.46
0.48
0.50
0.52
$M(\pi^+\pi^-)$ (GeV)
K_s°
(d)
300
200
100
0
-1
0
1
$\cos\theta_D^+$
Λ
(b)
EVENTS/(2 MeV)
1000
500
0
1.08
1.10
1.12
1.14
$M(p\pi^-)$ (GeV)
Λ
(e)
EVENTS/(0.1)
200
100
0
-1
0
1
$\cos\theta_D^+$
$\bar{\Lambda}$
(c)
200
100
0
1.08
1.10
1.12
1.14
$M(\bar{p}\pi^+)$ (GeV)
5-83
4393B10
$\bar{\Lambda}$
(f)
50
40
30
20
10
0
-1
0
1
$\cos\theta_D^+$

Fig. 2

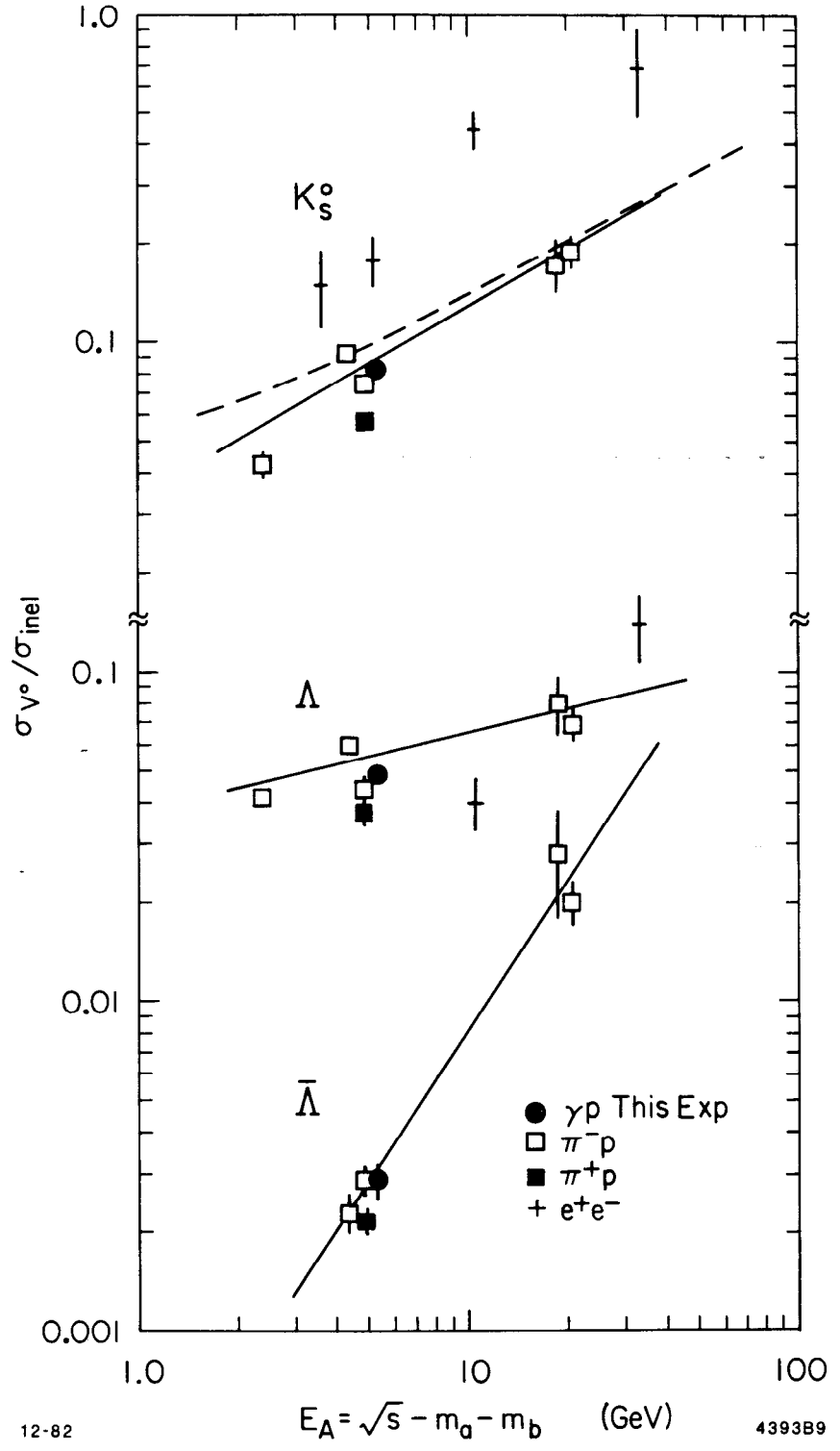
1.0
0.1
0.1
0.01
0.001
K^o_s
Λ
$\bar{\Lambda}$
$\sigma_{V^o}/\sigma_{inel}$
γp This Exp
π^-p
π^+p
e^+e^-
1.0
10
100
$E_A = \sqrt{s} - m_a - m_b$ (GeV)
12-82
4393B9

Fig. 3

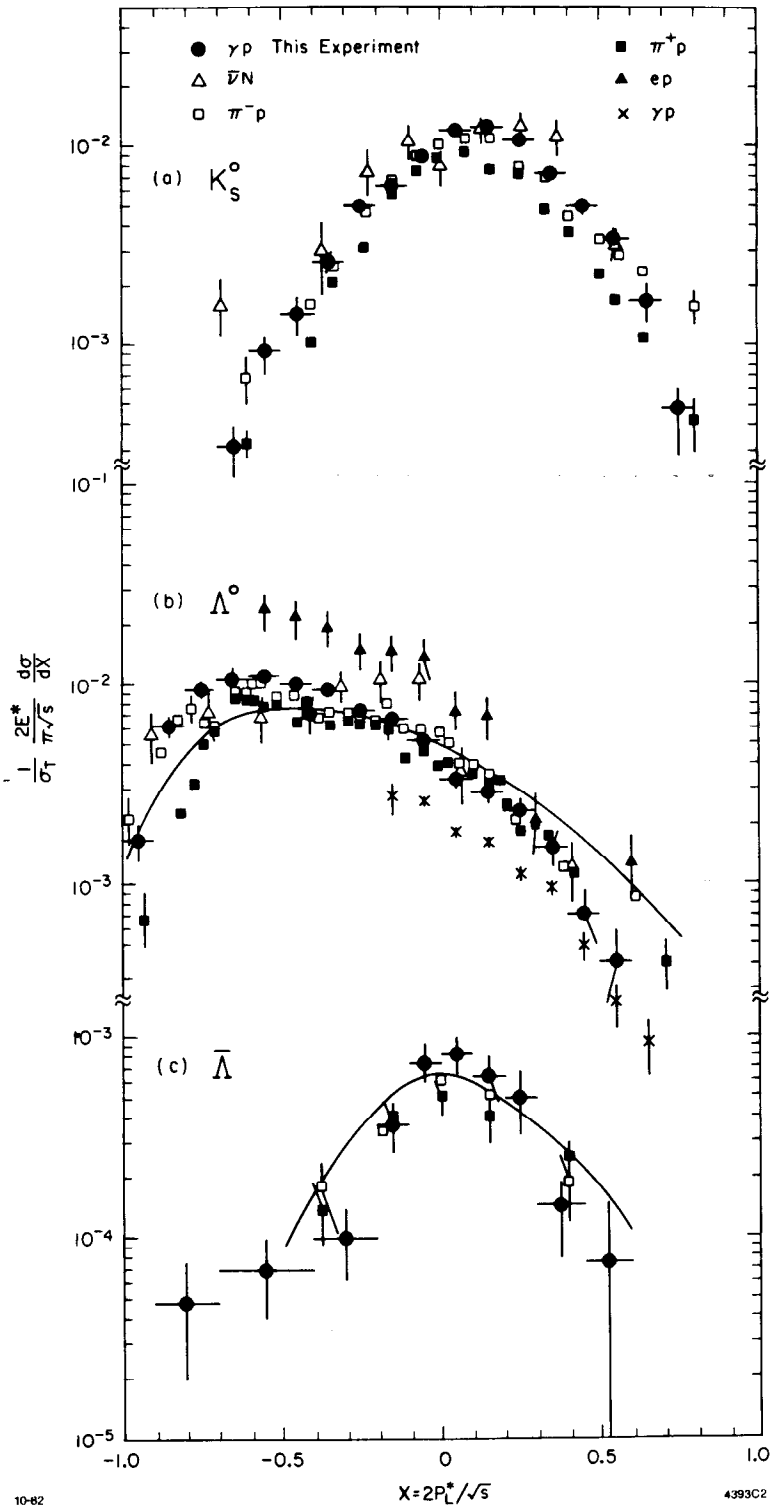
γp This Experiment
π⁺p
ν̄N
ep
π⁻p
γp
(a) K°S
(b) Λ°
(c) Λ̄
10⁻²
10⁻³
10⁻¹
10⁻⁴
10⁻⁵
-1.0
-0.5
0
0.5
1.0
X=2P*L/√s
10-82
4393C2

Fig. 4

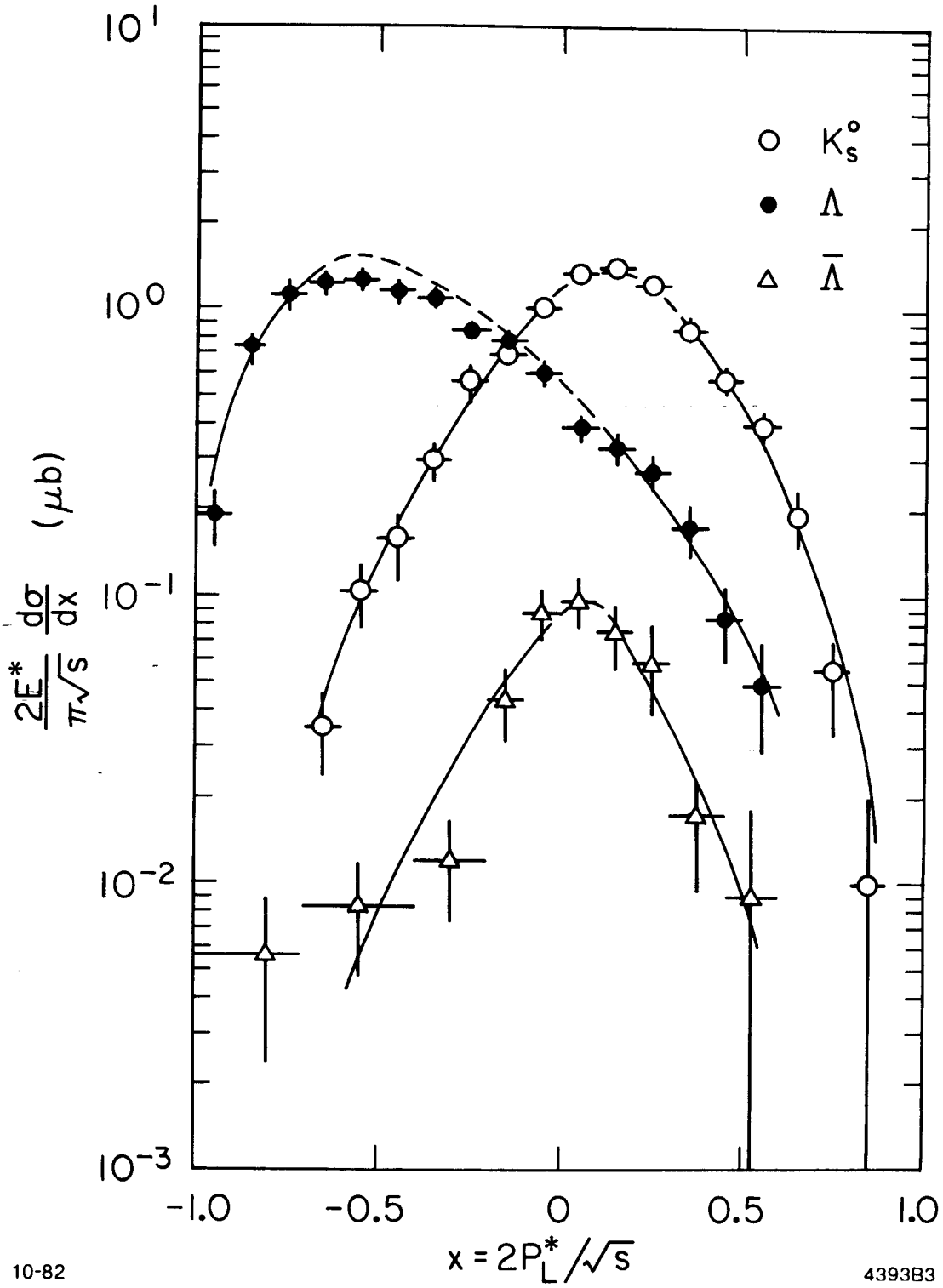
10^1
10^0
10^{-1}
10^{-2}
10^{-3}
$\frac{2E^*}{\pi\sqrt{s}}\frac{d\sigma}{dx}$ (μb)
K_s^o
Λ
$\bar{\Lambda}$
-1.0
-0.5
0
0.5
1.0
$x = 2P_L^*/\sqrt{s}$
10-82
4393B3

Fig. 5

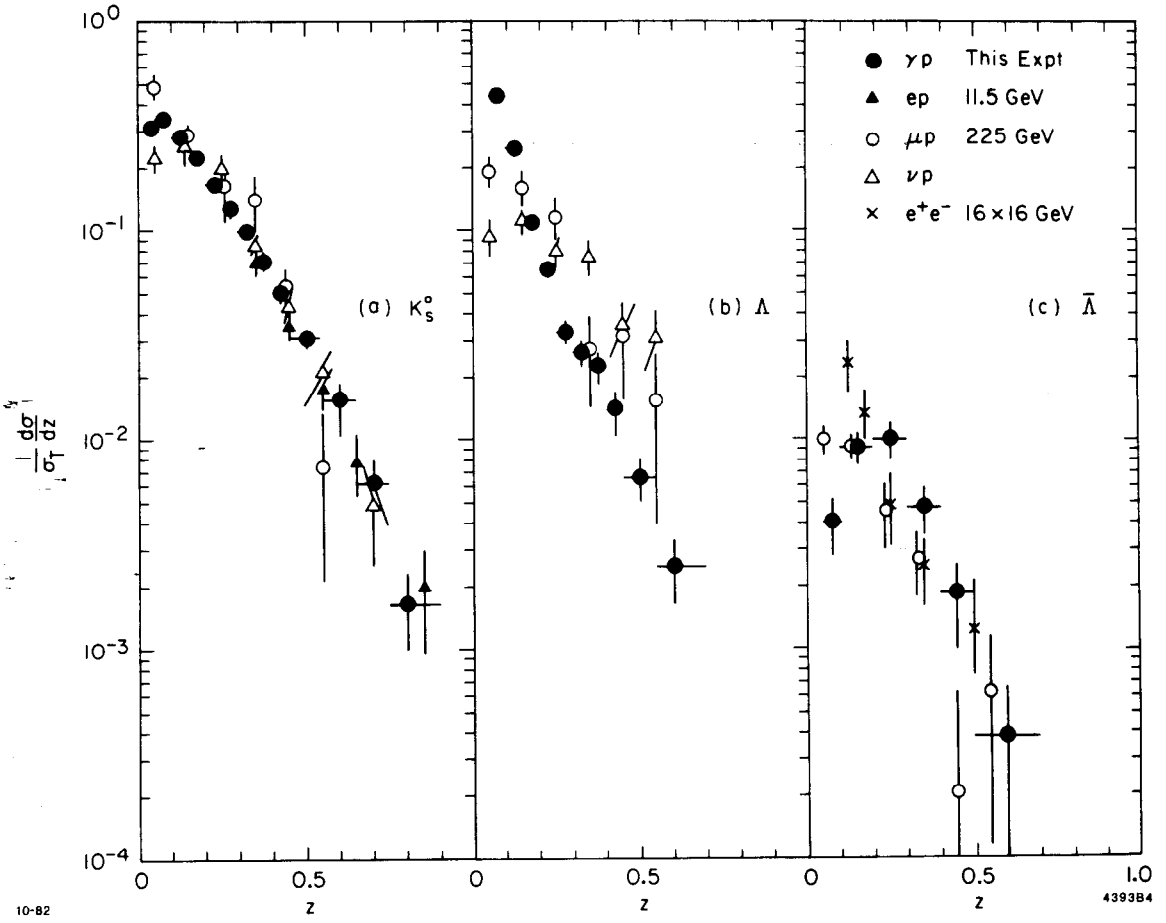
10^0
10^{-1}
10^{-2}
10^{-3}
10^{-4}
$\frac{1}{\sigma_T}\frac{d\sigma}{dz}$
(a) K^0_S
(b) Λ
(c) $\bar{\Lambda}$
γp This Expt
ep 11.5 GeV
μp 225 GeV
νp
e^+e^- 16×16 GeV
0
0.5
1.0
z
10-82
4393B4

Fig. 6

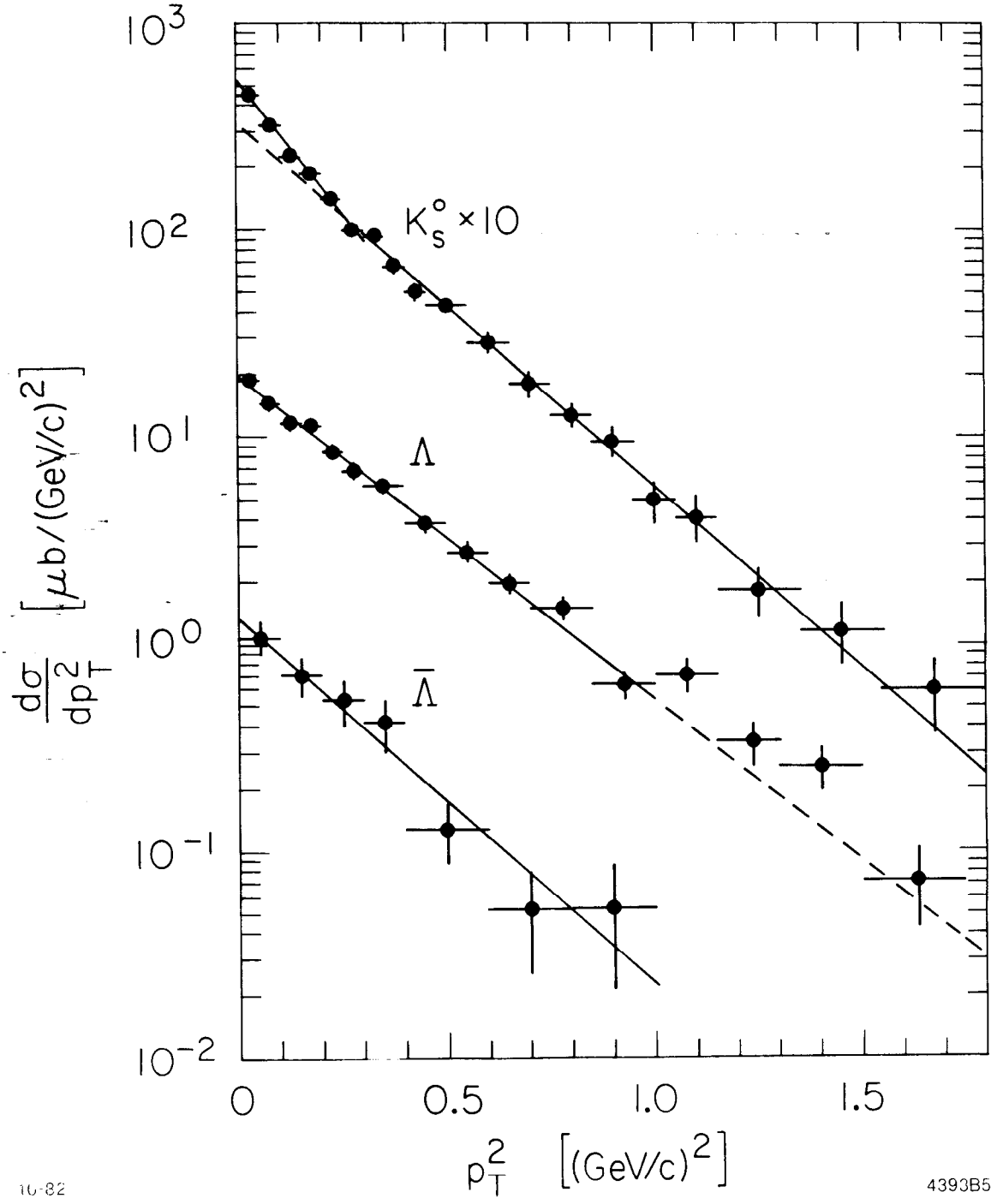
10^3
10^2
10^1
10^0
10^{-1}
10^{-2}
$K_s^o \times 10$
Λ
$\bar{\Lambda}$
$\frac{d\sigma}{dp_T^2}$ $[\mu b/(GeV/c)^2]$
0
0.5
1.0
1.5
p_T^2 $[(GeV/c)^2]$
4393B5

Fig. 7

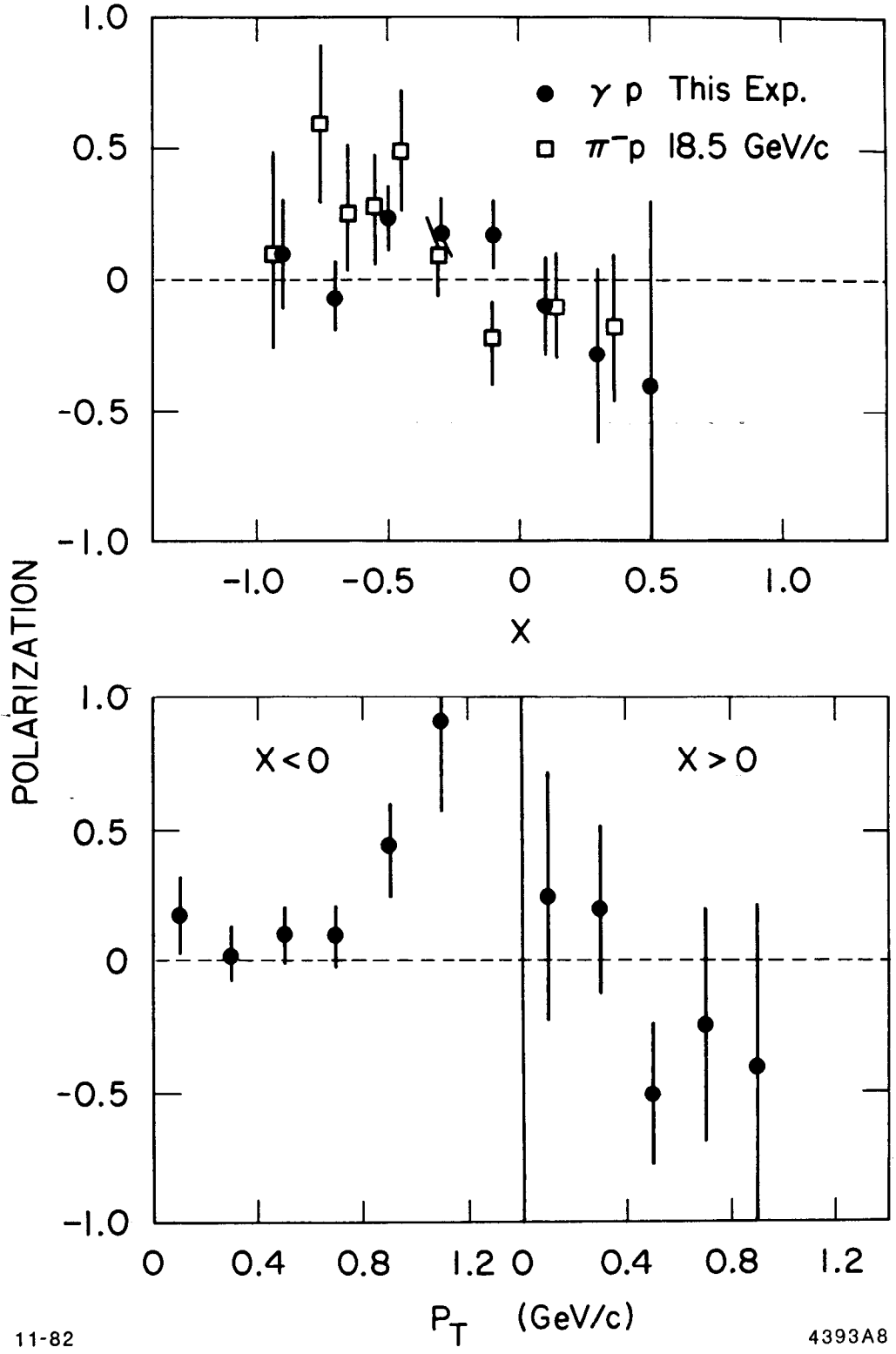
1.0
0.5
0
-0.5
-1.0
γ p This Exp.
π⁻p 18.5 GeV/c
-1.0
-0.5
0
0.5
1.0
X
POLARIZATION
X<0
X>0
0
0.4
0.8
1.2
P_T (GeV/c)
11-82
4393A8

Fig. 8

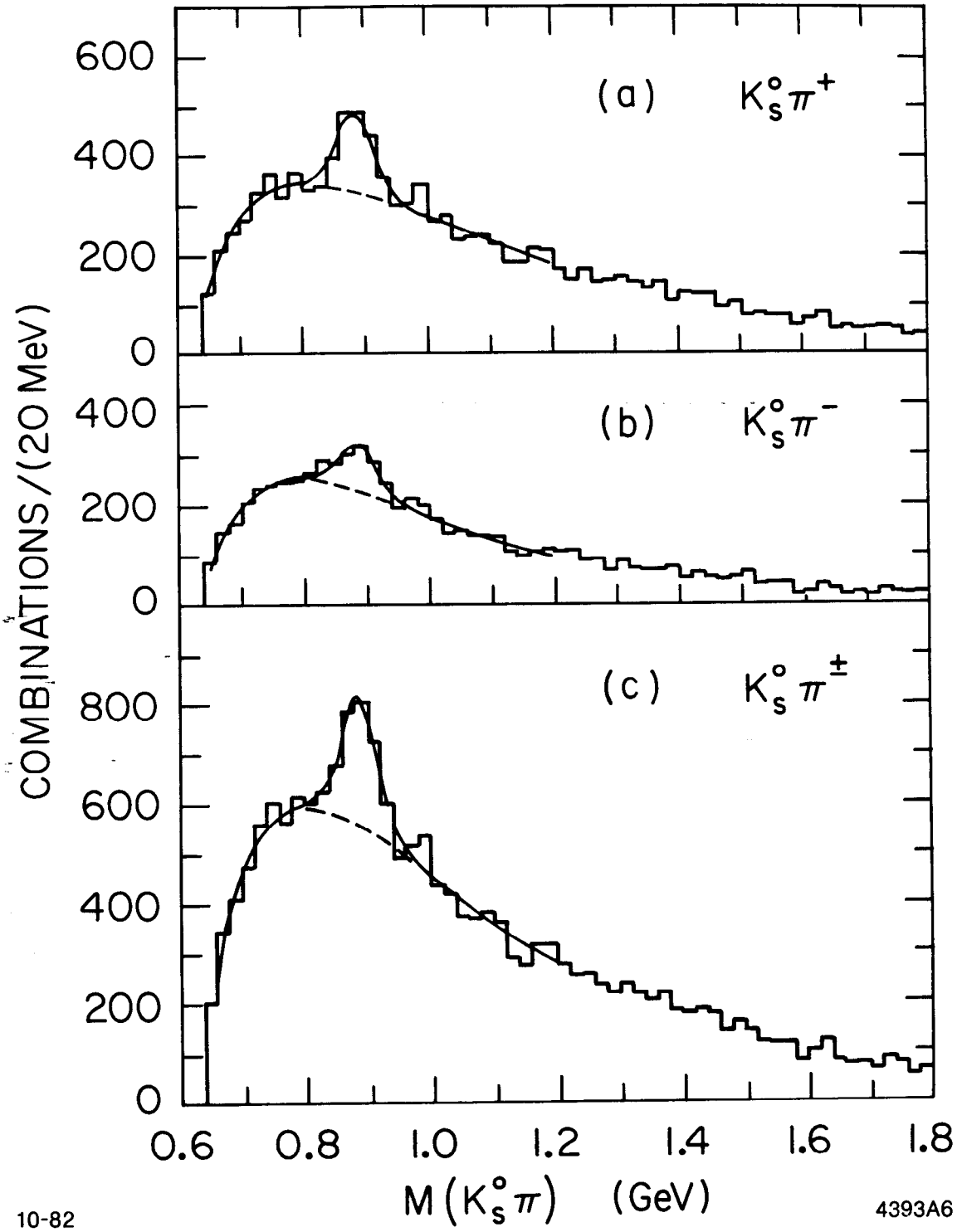
600
400
200
0
(a) $K^0_S\pi^+$
400
200
0
(b) $K^0_S\pi^-$
800
600
400
200
0
(c) $K^0_S\pi^\pm$
COMBINATIONS/(20 MeV)
0.6
0.8
1.0
1.2
1.4
1.6
1.8
$M(K^0_S\pi)$ (GeV)
10-82
4393A6

Fig. 9

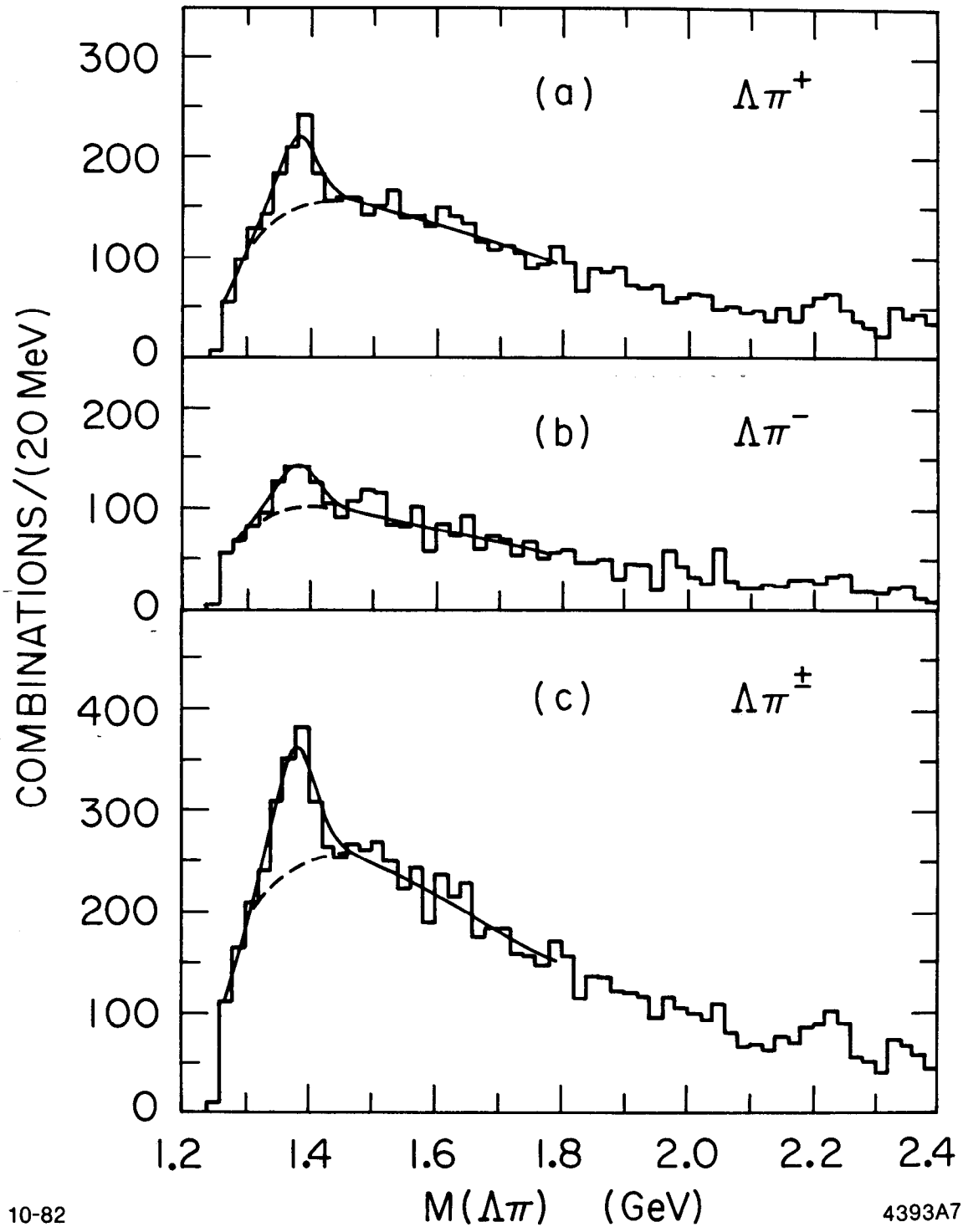
300
200
100
0
(a)
$\Lambda\pi^+$
200
100
0
(b)
$\Lambda\pi^-$
400
300
200
100
0
(c)
$\Lambda\pi^\pm$
COMBINATIONS/(20 MeV)
1.2
1.4
1.6
1.8
2.0
2.2
2.4
M(Λπ) (GeV)
10-82
4393A7

Fig. 10